JCAAC (2024), **1**, 15–24

METHODS & ALGORITHMS

Orbits of binary stars from lunar occultations

Enrique Velasco[1]

[1]Agrupación Astronómica de Madrid and Universidad Autónoma de Madrid, Spain. E-mail: enrique.velasco@uam.es.

Keywords: lunar occultations, double stars

Abstract
A method is presented to incorporate single observations of lunar occultations of binary stars into the calculation of their orbits. The standard method of orbit estimation, based on optimisation of a merit function, is designed to use two-dimensional astrometric measurements obtained observationally. In the present method the merit function is augmented to include an extra term, containing the one-dimensional solution extracted from the lunar occultation. Comparison between the two methods is provided, and it is shown that, in some circumstances, the partial information contained in one-dimensional solutions is enough to estimate orbits very close to those derived from fully two-dimensional sets of measurements. The method is discussed with an example based on a real binary star.

Resumen
Presentamos un método para utilizar las observaciones de ocultaciones lunares de estrellas dobles por parte de una única estación en el cálculo de las órbitas de estas estrellas. El método clásico de estimación de órbitas se basa en la optimización de una función de merito, y se utiliza sobre conjuntos de medidas astrométricas bidimensionales obtenidas mediante observaciones. El método que se presenta extiende la función de mérito para incluir un término extra, que contiene la solución unidimensionales obtenida a partir de la ocultación lunar. Se muestra una comparación entre los dos métodos, y se discute el resultado de que, en algunas circunstancias, la información parcial contenida en una solución unidimensional puede ser equivalente a la de una medida bidimensional para estimar la órbita. Se discute el método con un ejemplo de estrella binaria real.

1. Introduction

Lunar occultations have been extensively used since the '70s of the last century to detect duplicity in hitherto unknown binary stars [1, 2, 3] (as an example of recent work in binary stars and stellar diameters, see Ref. [4]). This technique is highly accurate and usually ranked at the same level as interferometric techniques. Under favourable circumstances projected distances between the components can reach accuracies of a few milliarcseconds (mas), competing with speckle interferometry using metre-sized telescopes. This level of accuracy can now be achieved even by dedicated amateur astronomers, which potentially increases the coverage of the large number of stars occulted by the Moon.

A crucial feature of a lunar occultation observation is that it only provides a one-dimensional astrometric observation for the binary star, instead of the full two-dimensional position required in orbit optimization techniques. Indeed, the time interval between the contacts of the two components only sets a constraint on the two angular coordinates $\boldsymbol{r} = (x, y)$, or (ρ, PA), of one component relative to the other ($\rho = |\boldsymbol{r}| = r$); see Fig. 1(a). In other words, only a lower bound for the separation between components can be derived, instead of the true separation ρ and position angle PA [5]. It is only when two or more observations of the same occultation from sufficiently separated observatories (probing different regions of the lunar

limb) are combined that a full astrometric solution may be derived. This situation can be achieved by groups of dedicated amateur observers working in coordination [6, 7], but represents a limitation for the widespread implementation of the lunar-occultation technique.

The condition of simultaneous observations of the same occultation can be relaxed, and results of two or more occultations of the same star in different lunations combined, to provide a complete astrometric solution. The epoch associated to this solution is assigned to the average epoch of observation. This procedure may be acceptable for long-period binary stars, provided the epochs of observation are not too distant and their time interval is much smaller that the period. An obvious problem arises in the case of binary stars of unknown period, or newly discovered binary stars. In this sense, unpaired one-dimensional solutions are in principle useless, and cannot be used in orbit optimization procedures.

In this paper we review a method of orbit estimation which uses both astrometric (x, y) positions (two-dimensional, or 2D astrometric solutions), typically obtained from standard astrometric techniques or paired lunar occultations, and one-dimensional (1D) solutions from unpaired lunar occultations. The method has been described before [8, 9, 10], but its use is not widespread. Here we present it in detail. The method allows to refine and correct previously estimated orbits and, for some stars, estimate new orbits for the first time. The large database of lunar occultations due to Herald and Gault [11] can be used to explore forgotten one-dimensional solutions, or to disentangle unduly combined solutions, which allows to refine a relatively large number of orbits of the *Sixth catalog of orbits of visual binary stars* (6Orb) [12].

The present article is a short introduction which intends to show the potential of the method. A more formal presentation and applications to actual data is left for future publications. The style of the article is pedagogic and an effort has been made to present the material in a self-contained way.

The article is arranged as follows. In Section 2 we define the geometry of a 1D linear solution, explaining how it is calculated and the uncertainties associated to the position of the solution. Section 3 is devoted to the standard method or orbit determination of binary stars, which is based on a least-squares method containing a set of 2D measurements. An extension of the merit function that includes 1D solutions from lunar occultations is presented in Section 4, and some general properties of this function are analysed. Section 5 presents the case of a particular double star where the addition of a 1D solution is seen to be relevant. Some conclusions are given in Section 6.

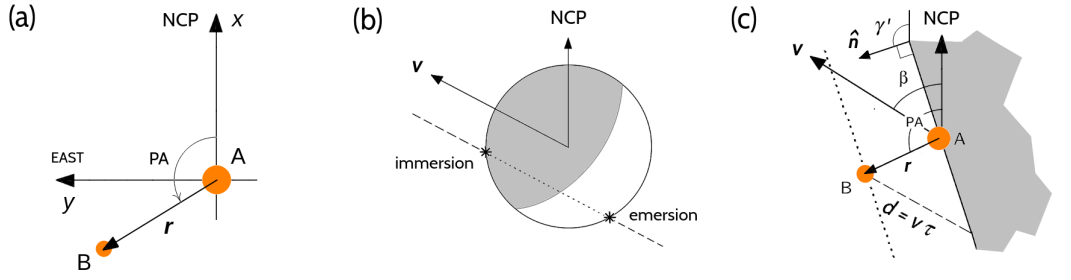

Figure 1. *(a) Definition of the celestial coordinate system xy for double-star work. It is centred at the primary component A, with axis x along the local celestial meridian towards the North Celestial Pole (NCP), and y axis along the local celestial parallel towards the East. The ρ (separation) and PA (position angle) coordinates are defined. The relation with the rectangular coordinates of the relative position vector* $\boldsymbol{r} = (x, y)$ *is given through the usual expressions* $x = \rho \cos PA$, $y = \rho \sin PA$. *(b) Geometry of a lunar occultation. The star traces a chord across the lunar disc, defining two occultation events: immersion and emersion.* $\boldsymbol{v}$ *is the topocentric apparent velocity of the Moon projected on the plane of the sky. (c) Local geometry of the immersion of a double star, with the A component having the first contact.*

2. One-dimensional solutions

Figs. 1(b) and (c) show the geometry of a lunar occultation. An immersion event is considered for the sake of concreteness. Panel (c) shows the specific geometry for a binary star, with components A (primary) and B (secondary). We assume A is occulted first but this assumption can be generalised easily (see later). The projected lunar limb is supposed to be a straight line (straight-limb approximation). The calculation of the straight line and the limitations of this approximation are discussed later. Note that the limb normal is at an angle γ' with respect to the NCP, but that the apparent velocity of the Moon (given by the angle β) is along a direction different (in general) from that of the limb normal. Therefore, by measuring the time interval τ between the two events, we only have information on the component of the separation between components along the limb normal. With the help of Fig. 1(c), it is easy to derive the following equation:

$$\boldsymbol{r}\cdot\hat{\boldsymbol{n}} = v\tau\hat{\boldsymbol{\beta}}\cdot\hat{\boldsymbol{n}}, \qquad (\boldsymbol{r} - v\tau\hat{\boldsymbol{\beta}})\cdot\hat{\boldsymbol{n}} = 0, \tag{2.1}$$

where $\hat{\boldsymbol{n}} = (\cos\gamma', \sin\gamma')$ is the limb normal at the contact point of A, v the topocentric apparent velocity of the Moon, and $\hat{\boldsymbol{\beta}} = (\cos\beta, \sin\beta)$. Note that $\boldsymbol{r}\cdot\hat{\boldsymbol{n}}$ is the projection of the star vector separation $\boldsymbol{r}$ along the local limb normal $\hat{\boldsymbol{n}}$. This is made to be equal to the projection of the displacement of the Moon on the same direction within the time interval τ, i.e. $v\tau\hat{\boldsymbol{\beta}}\cdot\hat{\boldsymbol{n}}$. Also, Eqn. (2.1) shows that the vector $\boldsymbol{r} - v\tau\hat{\boldsymbol{\beta}}$ points along the limb, and is therefore orthogonal to $\hat{\boldsymbol{n}}$.

One crucial point is how γ', or $\hat{\boldsymbol{n}}$ for that matter, is calculated. Due to the roughness of the lunar limb and the uncertainty in the current positions of the two stars, it is not possible to calculate the value of γ' rigorously. Therefore some approximations, discussed in the next paragraph, have to be made. Note that Eqn. (2.1) represents a straight line projected on the sky, since v and β can be extracted from the lunar ephemerides, and γ' can be approximated [13]. It gives a linear relation between the two components of the relative position vector $\boldsymbol{r}$, but not the values of the coordinates separately. Eqn. (2.1) will be called *1D solution*, as opposed to the determination of the full vector $\boldsymbol{r}$ (2D solution) achieved by application of the standard astrometric methods. Combination of two different observations,

$$\boldsymbol{r}\cdot\hat{\boldsymbol{n}}_1 = v_1\tau_1\hat{\boldsymbol{\beta}}_1\cdot\hat{\boldsymbol{n}}_1, \qquad \boldsymbol{r}\cdot\hat{\boldsymbol{n}}_2 = v_2\tau_2\hat{\boldsymbol{\beta}}_2\cdot\hat{\boldsymbol{n}}_2, \tag{2.2}$$

corresponding to two observations of the same occultation from two stations, leads to a unique solution for $\boldsymbol{r}$. When $M > 2$ observations are available, a least-square method can be applied:

$$S(\boldsymbol{r}) = \sum_{j=1}^{M}\left[\frac{(\boldsymbol{r} - v_j\tau_j\hat{\boldsymbol{\beta}}_j)\cdot\hat{\boldsymbol{n}}_j}{\sigma_j}\right]^2 \quad \longrightarrow \quad \text{min. w.r.t. } \boldsymbol{r}. \tag{2.3}$$

Eqn. (2.3) expresses a minimum condition over the sum of squares of the distances along the limb normals, extended over all observations, and leads to a 2×2 linear system of equations that can be solved analytically. σ_j is an uncertainty in the location of the straight line along the limb normals. When $M = 2$ both Eqns. (2.2) and (2.3) can be seen to lead to the same solution. A key step in the above calculation is how to estimate γ' and σ. Fig. 2 describes the process of how an average straight limb can be obtained by assuming the limb profile is rough at the scale of the (expected) separation between the two components ρ. Since the celestial coordinates of the two stars are not known in advance (otherwise the problem would be irrelevant), we need to have an estimate of the celestial position of A to be able to estimate the contact point on the lunar limb. Note that this problem would not be relevant if the limb were truly straight within some reasonable interval, as in panel (a). However, in the general case the limb will not be strictly linear.

The natural choice for the estimated coordinates is the catalogue coordinates (Gaia or otherwise), advanced to the epoch of observation, assuming a linear proper motion of the star. But this is only an

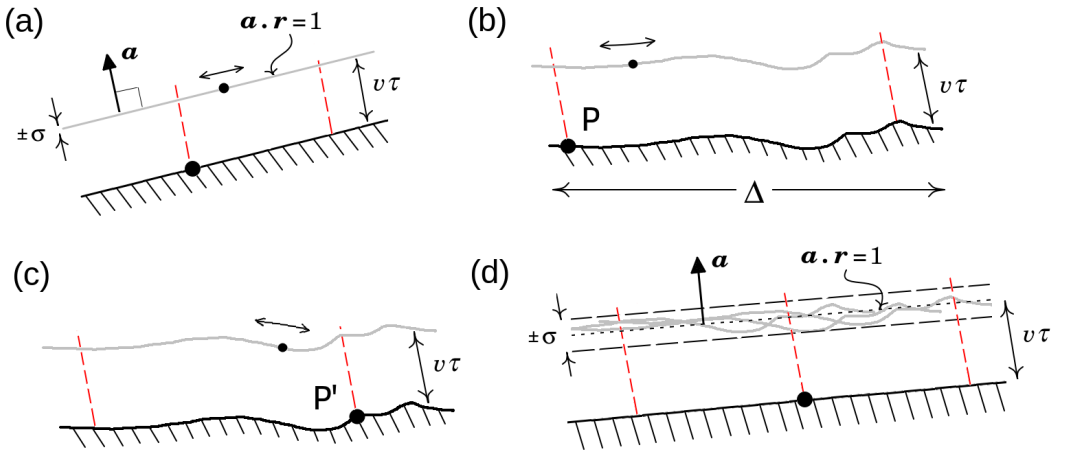

Figure 2. *Construction of the one-dimension solution for the lunar limb profile.*

approximation, as the internal motions of the binary star will cause the stars to be displaced from their catalogue positions. Using the estimated coordinates for A, and the estimated separation between the components, we can create an estimated landscape for the relevant lunar profile. This is shown in Fig. 2. The construction of an 'effectively linear' limb profile is based on the following argument. Assume the estimated coordinates for A lead to the contact point indicated by P in panel (b). The constraint imposed by the observation time interval τ implies that the B component will necessarily be at some point on a shifted limb (drawn in gray), which results by displacing the real limb a distance $v\tau$ in the direction of the apparent lunar motion. The resulting 'rough' 1D solution is identical to the actual limb, but shifted. Now, the uncertainty in the position of A forces us to probe other possible contact points, such as P′ in panel (c), finally resulting in a manifold of possible 'rough' 1D solutions, panel (d). The position of A should be displaced along the limb within some distance Δ, panel (b), which reflects the expected accuracy in the position of A. We can now use the set of shifted limbs to obtain both $\boldsymbol{a}$ and the uncertainty σ. In essence this procedure amounts to making a simple linear regression of the real limb within the interval Δ.

Let the resulting straight line be $c_1 x + c_2 y = d$. This can be written as

$$\boldsymbol{a} \cdot \boldsymbol{r} = 1, \quad \boldsymbol{a} = (a_x, a_y), \quad a_x = \frac{c_1}{d}, \quad a_y = \frac{c_2}{d}. \tag{2.4}$$

This representation is not numerically the most general, as it does not contain straight lines that pass through the origin. But such solutions are not physically admissible, as they correspond to situations where the two components are occulted at the same time (within observational accuracy). In practice a single vector $\boldsymbol{a}$ can represent acceptable solutions of arbitrary observational accuracy. Once $\boldsymbol{a}$ and σ are determined, we obtain $\hat{\boldsymbol{n}} = \boldsymbol{a}/a$, since $\boldsymbol{a}$ is a vector normal to the straight line.

In many cases the separation ρ will be so small compared with the typical length scales over which the lunar limb profile changes that the straight-limb approximation will be highly accurate. In some cases this will not be so, but the uncertainty will be controlled by the value of σ.

3. Standard orbit determination

In the standard method of binary-star orbit determination we have a set of 2D measurements, $\{\boldsymbol{r}_i\}$, $i = 1, \cdots, N$, at epochs $\{t_i\}$, with uncertainties σ_i (assuming both axes to be equivalent), and an orbit has to be determined. Let $\{P, T, e, a, i, \Omega, \omega\}$ be a set of orbital elements for the star (the Campbell elements), which we wish to determine. We remind the reader about the meaning of the elements [5]: P is the orbital period; T is the epoch of periastron; e is the eccentricity; a is the semimajor axis; i is the inclination; Ω is the longitude of the ascending node; and ω is the argument of periastron.

Given values for the orbital elements, the trajectory is given by a Keplerian function $\boldsymbol{r} = \boldsymbol{r}(P, T, e, a, i, \Omega, \omega; t)$ for epoch t. A merit function is defined as

$$S(P, T, e, a, i, \Omega, \omega) = \sum_{i=1}^{N} \left| \frac{\boldsymbol{r}_i - \boldsymbol{r}(P, T, e, a, i, \Omega, \omega; t_i)}{\sigma_i} \right|^2, \tag{3.1}$$

which is minimised with respect to the seven orbital elements. It is convenient to use the Thiele-Innes elements, A, F, B and G, instead of the Campbell elements a, i, Ω, ω. The relation between the two sets of elements is given by

$$\begin{aligned} A &= a(\cos\omega\cos\Omega - \sin\omega\sin\Omega\cos i) \\ B &= a(\cos\omega\sin\Omega + \sin\omega\cos\Omega\cos i) \\ F &= -a(\sin\omega\cos\Omega + \cos\omega\sin\Omega\cos i) \\ G &= -a(\sin\omega\sin\Omega - \cos\omega\cos\Omega\cos i). \end{aligned} \tag{3.2}$$

As a shorthand notation, let us define $\eta \equiv \{P, T, e, A, F, B, G\}$, and the matrix

$$\boldsymbol{\Theta} = \begin{pmatrix} A & F \\ B & G \end{pmatrix}. \tag{3.3}$$

Then $\boldsymbol{r}(\eta; t) = \boldsymbol{\Theta} \cdot \boldsymbol{r}_{\rm o}(t)$, where $\boldsymbol{r}_{\rm o} = (x_{\rm o}, y_{\rm o})$ is the position in the orbital plane. This is calculated as $x_{\rm o} = \cos\psi - e$, $y_{\rm o} = \sqrt{1-e^2}\sin\psi$, with ψ the eccentric anomaly, solution to the Kepler equation $\psi = m + e\sin\psi$, and $m = 2\pi(t-T)/P$ the mean anomaly for the epoch of calculation t. Eqn. (3.1) can be written as a quadratic form in $\boldsymbol{\theta}$,

$$S(\{P, T, e\}; \boldsymbol{\theta}) = \frac{1}{2}\sum_{i=1}^{N} \boldsymbol{\theta}\cdot\boldsymbol{M}\cdot\boldsymbol{\theta} - \boldsymbol{n}\cdot\boldsymbol{\theta} + n_0, \tag{3.4}$$

where $\boldsymbol{\theta} = (A, F, B, G)$, $\boldsymbol{M}$ is a 4×4 matrix,

$$\boldsymbol{M} = \left(\begin{array}{c|c} \boldsymbol{\Lambda} & \boldsymbol{0} \\ \hline \boldsymbol{0} & \boldsymbol{\Lambda} \end{array}\right), \quad \boldsymbol{\Lambda} = \sum_{i=1}^{N} \frac{\boldsymbol{r}_{oi}\boldsymbol{r}_{oi}}{\sigma_i^2}, \tag{3.5}$$

and

$$\boldsymbol{n} = (\mu_{11}, \mu_{12}, \mu_{21}, \mu_{22}), \qquad \boldsymbol{\mu} = \sum_{i=1}^{N} \frac{\boldsymbol{r}_{{\rm o}i}\boldsymbol{r}_i}{\sigma_i^2}, \qquad n_0 = \frac{1}{2}\sum_{i=1}^{N} \frac{|\boldsymbol{r}_i|^2}{\sigma_i^2}. \tag{3.6}$$

Note that $\boldsymbol{\mu}$ is also a matrix, and its definition contains sums of dyadic products.

3.1. Minimization and estimation of orbital parameters

Eqn. (3.4) naturally leads to a minimization strategy where S is first minimised with respect to $\boldsymbol{\theta}$, for fixed values of $\{P, T, e\}$:

$$\nabla_{\boldsymbol{\theta}} S = \mathbf{0} \quad \rightarrow \quad \boldsymbol{M} \cdot \boldsymbol{\theta} = \boldsymbol{n}, \quad \boldsymbol{\theta} = \boldsymbol{\theta}(P, T, e) = \boldsymbol{M}^{-1} \cdot \boldsymbol{n}, \tag{3.7}$$

which leads to an effective function,

$$\widetilde{S}(P, T, e) \equiv S(P, T, e; \{\boldsymbol{c}(P, T, e)\}), \tag{3.8}$$

with $\boldsymbol{\theta}(P, T, e)$ given by Eqn. (3.7). The function $\widetilde{S}(P, T, e)$ can be minimised by various methods. The most popular method is the search-grid method of Hartkopf et al. [14], but Monte Carlo methods are also routinely used. In the search-grid method, the function $\widetilde{S}$ is evaluated on a small grid about a point with initial values (P, T, e), and the minimum detected. A new grid is defined about the minimum, and the process Here we use a slightly different approach, which consists of the following. For fixed value of e in some interval $[e_1, e_2]$ (where $e_1 \sim 0$ but finite, and $e_2 \sim 1$ but $e_2 < 1$), we calculate $\widetilde{S}$ in the plane (P, T), using the relation $\widetilde{S}(P, T, e) = \widetilde{S}(P, T + P, e)$ and $P \in [P_1, P_2]$, $T \in [T_1, T_1 + P]$. Values for P_1, P_2 and T_1 are set by a trial and error process. The minimum of $\widetilde{S}$ with respect to P, T can be calculated approximately using a grid, and then refined using a steepest descent method. This is done for all e in the above interval, and a one-dimensional minimisation is then performed with respect to e.

3.2. Estimation of uncertainties

As in all statistical methods, uncertainties in the calculated values must be provided. A look at the quadratic equation given by Eqn. (3.4) suggests that the inverse of the $\boldsymbol{M}$ matrix provides a covariance matrix, $\boldsymbol{C} = \boldsymbol{M}^{-1}$. The square of the diagonal elements of $\boldsymbol{C}$ give estimates for the Thiele-Innes elements:

$$\sigma_A = \sqrt{C_{11}}, \quad \sigma_F = \sqrt{C_{22}}, \quad \sigma_B = \sqrt{C_{33}}, \quad \sigma_G = \sqrt{C_{44}}. \tag{3.9}$$

Uncertanties in the angular Campbell elements follow from the latter using Eqns. (3.2). Uncertainties for the remaining elements, P, T, e, can be obtained from the grid step [14]. A more formal method is to apply error propagation using $\boldsymbol{\theta} = \boldsymbol{M}^{-1} \cdot \boldsymbol{n}$. However, this method implicitely assumes that the function S is quadratic in all the elements, but this is generally not true. Alternatively, in these cases obe can apply the method based on confidence levels [15]. Uncertainties may vary depending on the method used. In the following we use the method based on the grid size.

4. Orbit determination using 1D solutions

In the extended method we add the contributions from the possibly multiple 1D solutions at epoch t_j. We define the augmented function

$$S(\{P, T, e\}; \boldsymbol{\theta}) = \sum_{i=1}^{N} \left| \frac{\boldsymbol{r}_i - \boldsymbol{r}_i^{(\mathrm{o})}}{\sigma_i} \right|^2 + w \sum_{j=1}^{M} \left(\frac{\boldsymbol{a}_j \cdot \boldsymbol{r}_j - 1}{\sigma'_j} \right)^2, \tag{4.1}$$

where j runs over the M 1D (straight-line) solutions at times τ_j, and $\sigma'_j = \sigma_j / a$. The extra term depends functionally on $\{P, T, e\}, \boldsymbol{\theta}$ through $\boldsymbol{r}$. w is the relative weight between the 2D and 1D solutions (in the

following we take $w = 1$). Eqn. (4.1) can also be written as (3.4), with

$$\boldsymbol{M} = \left(\begin{array}{c|c} \boldsymbol{\Lambda} + \boldsymbol{\Pi}_{11} & \boldsymbol{\Pi}_{12} \\ \hline \boldsymbol{\Pi}_{21} & \boldsymbol{\Lambda} + \boldsymbol{\Pi}_{22} \end{array} \right), \quad \boldsymbol{\Pi}_{lm} = \sum_{j=1}^{M} \frac{a_j^{(l)} r_{\mathrm{o}j}^{(m)} \boldsymbol{a}_j \boldsymbol{r}_{\mathrm{o}j}}{\sigma_j'^2}, \tag{4.2}$$

and

$$\boldsymbol{n} = (\mu_{11} + \lambda_{11}, \mu_{12} + \lambda_{12}, \mu_{21} + \lambda_{21}, \mu_{22} + \lambda_{22}), \quad \lambda = \sum_{j=1}^{M} \frac{\boldsymbol{a}_j \boldsymbol{r}_{\mathrm{o}j}}{\sigma_j'^2}. \tag{4.3}$$

In Eqn. (4.2) components of $\boldsymbol{a}_j$ and $\boldsymbol{r}_{\mathrm{o}j}$ are denoted by superscripts. In problems without 1D solutions, we can take $a_j = 0$, and the standard case is recovered. The solution $\boldsymbol{\theta}$ is also given by a linear system of equations, as in the standard case.

Because of the presence of $\boldsymbol{\Pi}_{ij}$, the elements of $\boldsymbol{\theta}$ are not decoupled, and the full 4×4 linear system has to be solved, which can be done analytically (the expressions are too long to be written here). Gauss elimination can also be used to obtain the solution. Once this is calculated, the function S is minimised in a nested iteration, as in the previous section. This is what we call *method I*.

An alternative procedure, *method II*, is to minimise only the first term in Eqn. (4.1) for each set (P, T, e), as in the standard procedure, to obtain the Thiele-Innes elements, and then minimise the whole function S in a nested iterative process, using the same strategy as before. This amounts to using (3.1) instead of (4.1) to calculate $\boldsymbol{\theta}$. Both these methods lead to the same solution, but the first should be preferred when the arc of measurements is very short. Uncertainties in the elements can be estimated as in the standard method.

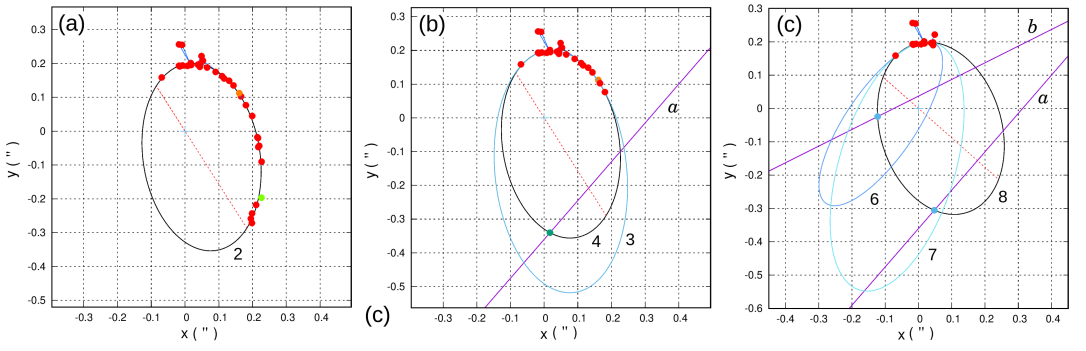

Figure 3. *1D and 2D measurements and orbits fitted to different sets of data for WDS J04422+2257Aa,Ab. 2D measurements are taken from the Fourth Interferometric Catalog [17]. Dotted red lines are the apsis lines. (a) Full set of 36 2D measurements, covering an arc close to* 180°*, and fitted orbit, Set 2. (b) A subset of 25 2D measurements, covering an arc about* 90° *wide, and the 1D solution obtained from a lunar occultation [7] (J2022.0), with label a. The orbits fitted to Sets 3 and 4 are shown. The green filled circle is the position along the optimised orbit using Set 4 at J2022.0. (c) A subset of 15 2D measurements, covering* ∼ 50°*, and two 1D solutions: a is the same solution as in (b), while b is a fictitious solution that goes through a position obtained from the best orbit (Set 2) at J2033.0. Orbits fitted to Sets 6, 7 and 8 are shown. Blue circles indicate the positions along the optimised orbit (Set 8) at epochs J2022.0 and J2033.0.*

5. An example: WDS J04422+2257Aa,Ab

We take the binary star WDS J04422+2257Aa,Ab as an example. Discovered in 1980 and last observed in 2007, a grade-3 orbit was computed for this star, based on 36 observations, by Cvetković and Novaković [16] in 2010. The orbit has been recalculated, and Fig. 3(a) shows the projected orbit, with the 36 measurements included. Table 1 summarises the values of the orbital elements in the different conditions. Set 1 corresponds to the published orbit, while Set 2 is our recalculated orbit (deduced from the same dataset, but using uncertainties which may be slightly different from the ones used in [16]). This orbit will be called *reference orbit* in the following.

As a test, we reproduced a situation with a fewer number of observations by limiting the number of measurements to 25, as drawn in Fig. 3(b). The resulting orbit is represented in blue. Set 3 in Table 1 pertains to this case. This orbit is quite far from the reference orbit (in black), since the first 25 measurements cover a short arc (approximately 90°), while the full set of data covers approximately 180°.

Also represented in Fig. 3(b) is the orbit resulting by adding the 1D solution from the results of a lunar occultation occurred on 17 December 2021 [7] to the set of 25 measurements. We can see that it is almost indistinguishable from the reference orbit (see Set 4 in Table 1): despite containing only partial astrometric information, the 1D solution correctly constraints the orbit. We can see that Sets 3 & 4 are practically identical, but Set 4 spans an arc of 2D measurements which is half that used in Set 3.

To understand this result and why the 1D lunar limb represents a strong constraint, let us consider method II. At each step of the iterative process one first generates an orbit from the 2D measurements using S as the objecive function. The S function is then evaluated, and the trial values for $\{P, T, e\}$ are changed along a direction towards the minimum. Note that S is sensitive to the distance from the predicted orbital positions at τ_j to the straight lines given by $\boldsymbol{a}_j \cdot \boldsymbol{r}_j = 1$. Obviously the process will tend to minimise these distances in conjunction with the distances from the orbit to the 2D measurements. Unless the trial orbit is very far from the optimal one, the process should be smoothly driven to the correct minimum and therefore to the optimal orbital elements.

Now we show that, in favourable cases, 1D solutions may lead to orbits of similar quality as 2D measurements. Consider the same example as before (Set 4 in Table 1), but now we replace the 1D solution of Fig. 3(b) by the 2D position indicated by the green circle. After orbit optimisation with the 25 + 1 2D measurements (25 real and 1 fictitious), we arrive at Set 5, which is very close to Set 4. In this case *the 1D solution is as accurate as the 2D solution as regards orbit optimisation!*

Fig. 3(c) shows a more strict case, where only 15 2D measurements, spanning an arc $\sim 50°$ long, are used. The orbit that results from these 2D solutions is quite far from optimal, Set 6 in Table 1. The orbit improves when the 1D solution is considered, Set 7. By including a second 1D solution (a fictitious observation chosen such that the limb intersects the reference orbit precisely at the orbital point associated to the epoch of observation, J2033.0), conveniently located in a region void of measurements, the resulting orbit, Set 8, is reasonably close to the reference orbit. Again, 1D solutions consistently improve orbits based on short arcs.

As an additional check, we consider the full set of 2D observations, and compare cases where only one or the two 1D solutions are added. In both cases the improvement is not substantial (see Fig. 3(d) and Table 1). This means that the published orbit is quite robust (and perhaps would deserve a lower grade).

Needless to say, there are situations where 1D solutions may not lead to unique or reasonable orbits. Spurious solutions will result when combining short arcs and particular configurations of the straight line. In these cases, solutions should always be analysed for possible erroneous orbits, and the initial guess for the orbit should be chosen using a conditioning strategy based e.g. on Monte Carlo sampling.

Table 1. *Orbital elements, P, T, e, a, A, F, B and G that result from optimisations made with different sets of data for WDS J04422+2257Aa,Ab. The combination of 2D and 1D solutions for each set is given in Column 'Data'. Set 1 corresponds to the published orbit [16]. In all cases starting values for the search grid method were $P = 60$ y, $T = J2050.0$, and $e = 0.2$.*

Set	Data 2D+1D	P (y)	T (y)	e	a (″)	A (″)	F (″)	B (″)	G (″)	O−C* (″)
1**	36 + 0	57.896	2037.956	0.357	0.284	−0.2157	−0.1293	−0.1841	+0.1335	–
2	36 + 0	57.219 ±0.005	2037.094 ±0.005	0.365 ±0.0005	0.287 ±0.002	−0.2101 ±0.0025	−0.1940 ±0.0026	−0.1340 ±0.0025	+0.1233 ±0.0026	0.011
3	25 + 0	85.344 ±0.005	2066.594 ±0.005	0.484 ±0.0005	0.368 ±0.007	−0.3292 ±0.0067	−0.1648 ±0.0046	−0.1024 ±0.0067	0.1938 ±0.0046	0.016
4	25 + 1	58.734 ±0.005	2038.547 ±0.005	0.370 ±0.0005	0.288 ±0.008	−0.2112 ±0.0060	−0.1943 ±0.0030	−0.1342 ±0.0060	0.1239 ±0.0030	0.011
5†	26 + 0	58.141 ±0.005	2038.094 ±0.005	0.352 ±0.0005	0.283 ±0.007	−0.2136 ±0.0055	−0.1844 ±0.0031	−0.1269 ±0.0055	0.1311 ±0.0031	0.017
6	15 + 0	35.953 ±0.005	2095.562 ±0.005	0.735 ±0.0005	0.403 ±0.007	−0.0616 ±0.0129	0.3521 ±0.0122	0.1541 ±0.0129	−0.1531 ±0.0122	0.153
7	15 + 1	79.969 ±0.005	2065.953 ±0.005	0.482 ±0.0005	0.389 ±0.006	−0.3611 ±0.0107	0.1110 ±0.0156	0.1334 ±0.0107	0.1720 ±0.0156	0.049
8+	15 + 2	57.234 ±0.005	2035.859 ±0.005	0.387 ±0.0005	0.2754 ±0.0215	−0.1534 ±0.0160	−0.2257 ±0.0068	−0.1737 ±0.0160	0.0852 ±0.0068	0.015

* Per point. Includes all 36 measurements.
** Published orbit [16].
† One 2D point, at J2022.0, is a fictitious measurement.
+ One of the two 1D solutions, at J2033.0, is a fictitious measurement.

6. Conclusions

One-dimensional solutions for the relative astrometry of a binary star may be incorporated into standard procedures of orbit optimisation. In some cases the contribution from these solutions may be as accurate as those from standard two-dimensional astronometry. As noted by Mason [8], 1D solutions may be particularly relevant for epochs close to periastron, where the relative positions are changing more rapidly. Because of their relevance for binary-star astrometry, we urge the amateur community to undertake this type of measurements and to report the results [7].

We are presently analysing a large number of binary stars for which one or more 1D solutions are available, in an effort to improve or recalculate their orbital elements using the information obtained from lunar occultations. Also, an ongoing investigation, based on synthetic orbits, is exploring the landscape of possible situations and their relevance for orbit estimation. These results will be published elsewhere.

Acknowledgements

We thank Rachel Matson (USNO) for her help in providing data of the WDS catalogue for this investigation.

References

[1] R. E. Nather and D. S. Evans, Astron. J. **75**, 575 (1970).
[2] R. E. Nather and M. M. McCants, Astron. J. **75**, 963 (1970).

[3] R. E. Nather and D. S. Evans, Astrophys. and Space Sci. **11**, 28 (1971).
[4] L. Zampieri, A. Richichi, G. Naletto, C. Barbieri, A. Burtovoi, M. Fiori, A. Glindemann, G. Umbriaco, P. Ochner, V. V. Dyachenko and M. Barbieri, Astron. J. **158**, 176 (2019).
[5] See e.g. *Double Stars*, W. D. Heintz (Reidel Publishing, 1978) for a general introduction to double stars.
[6] https://occultations.org/
[7] https://sites.google.com/aam.org.es/oled/
[8] B. D. Mason, Astron. J. **112**, 2260 (1996).
[9] G. H. Schaefer, M. Simon, T. L. Beck, E. Nelan, and L. Prat, Astron. J. **132**, 2618 (2006).
[10] G. H. Schaefer, L. Prato, M. Simon, and J. Patience, Astron. J. **147**, 147 (2014).
[11] D. Herald and D. Gault,
http://vizier.cds.unistra.fr/viz-bin/VizieR?-meta.foot&-source=VI/132B
[12] http://www.astro.gsu.edu/wds/orb6.html
[13] Note that light curves containing diffraction fringes provide a length scale from which the value of γ' can be derived if v and β are known. This is not possible for step-like light curves, resulting from low frequency sampling typical of amateur work, which is the case in the present discussion.
[14] W. I. Hartkopf, H. A. McAlister, and O. G. Franz, Astron. J. **98**, 1014-1039 (1989).
[15] William H. Press et al., Numerical Recipes in C. The Art of Scientific Computing, 2nd Edition (Cambridge Univerty Press, 1992).
[16] Z. Cvetković and B. Novaković, Astron. Nachr. **331**, 304 (2010).
[17] http://www.astro.gsu.edu/wds/int4.html